JOURNAL OF SPACECRAFT AND ROCKETS
Vol. 42, No. 4, July–August 2005

Optimization of a Tetrahedral Satellite Formation

Daniel Chavez Clemente* and Ella M. Atkins†
University of Maryland, College Park, Maryland 20742

Two fundamental approaches can be applied to satellite-formation mission design: active control, where satellites exert forces with their thrusters to maintain a constant or periodic geometry for all or part of each orbit, and natural, where satellite orbits are designed to naturally assemble a geometry for all or part of each orbit to within a tolerance defined from scientific requirements. An actively controlled formation can be labeled virtual rigid body (VRB) because geometry is precisely maintained as if the satellites were rigidly connected. This work describes a hierarchical optimization method for minimizing mission design computational complexity and applies this method to the design of VRB, natural-orbit, and multi-impulse solutions for a tetrahedron formation applicable to the proposed magnetospheric multiscale mission. Cost is defined in terms of total fuel per second of observation and tetrahedron geometric quality factor. Although both natural-orbit and active solutions are feasible, the active solutions substantially increase average data quality and observation time per orbit at minimum fuel cost, and the multi-impulse solution does not require thruster use during data collection periods.

Nomenclature

$a, e, i, \Omega, \omega, \nu$	=	orbital elements of T, km, –, rad, rad, rad, rad
D_k	=	coordinate frame of kth satellite
$F(x_i)$	=	objective function evaluated at point x_i
$\boldsymbol{h}$	=	angular momentum vector
J	=	cost function with weighting factors w_1, 1/s; w_2, 1/s; w_3, s^2/km
n_{new}	=	number of recalculated points for optimization algorithm
Q_G	=	glassmeier quality factor
Q_R	=	Robert–Roux quality factor
$\boldsymbol{r}_{a,i}$	=	apogee position vector of ith satellite, km
${}^T\boldsymbol{r}_V$	=	position vector of frame V expressed in frame T, km
T	=	target reference coordinate frame
T_{obs}	=	observation time per orbit, h
V	=	vehicle coordinate frame with offset (V_x, V_y, V_z) from T
λ	=	active control region width, rad
μ	=	gravitational parameter of central body (Earth), km^3/s^2
ξ	=	angle from perigee to center of active control region, rad
ρ_i	=	orientation of the natural orbit plane of the satellite i, rad

Introduction

SPACECRAFT formation flight has broad applications in science, engineering, and defense. Formations are required for simultaneous measurements from multiple stations and increase reliability when redundant. Several formation-flying missions have been proposed or flown. A joint mission between LandSat-7 and EO-1 has proven the feasibility of autonomous formation flying, with the Autocon™ software[1] aboard EO-1 capable of maintaining the spacecraft within 450 km of Landsat-7. Two missions of particular relevance to this work are Cluster II,[2] launched in 2000, and the proposed magnetospheric multiscale (MMS) formation flight mission.[3,4] Both use a four-satellite regular tetrahedron geometry (i.e., a tetrahedron with equal edge lengths) to study Earth's magnetosphere. Cluster II is designed as a nonpermanent formation with spacecraft orbits that periodically form a tetrahedron. The goal of MMS is to study small-scale processes that occur in the magnetosphere and how these define and control its large-scale characteristics, as well as the structure of its different regions. To acquire the best science data, measurements must be taken by a three-dimensional cluster of four spacecraft in a tetrahedral arrangement, with an alternative configuration consisting of a five-spacecraft hexahedral array. Tetrahedron-based MMS mission design is currently under way, and nonpermanent Earth-orbiting designs based strictly on natural spacecraft orbits have been proposed.[5,6]

Formation mission designs may be categorized as either natural or actively controlled. Natural formations capitalize on the motion of spacecraft under central-body gravitational forces to maintain certain geometries for at least a segment of a circular or elliptical orbit. The satellites in these formations do not use propellants to control their positions, and so formation shape generally varies over time. The natural category also includes formations that naturally maintain a fixed geometry from the perspective of an observation target, such as a constant circular projection on the Earth's surface.[7] Such natural formations may still require active orbit correction to counter disturbances or unmodeled perturbations, but associated corrections typically have small magnitude and may be applied infrequently. Actively controlled formations, on the other hand, are those in which individual satellites are expected to apply thruster forces to maintain a prescribed geometry. As an example, multispacecraft variable-baseline interferometry mission designs have been proposed that require low-level active thrust to follow a trajectory that differs slightly from that imposed by gravitational forces.[8–10] The primary design goal for actively controlled formations is to avoid costly propellant usage although meeting formation geometric constraints, a particularly challenging task for low Earth orbit formations. To optimize the overall mission, the tradeoff between fuel expenditure (favoring natural formations) and accuracy (favoring actively controlled formations) must be quantified. This requires a comparison of the best natural with the best actively controlled solutions for each formation geometry and orbit that meet scientific objectives.

The problem of formation mission design has been extensively studied, ranging from the early analytical designs for circular orbits[11] to complex numerical optimizations for both inertial (e.g., flat-space) and orbiting missions. At the highest level of abstraction,

Received 2 April 2004; revision received 30 July 2004; accepted for publication 30 July 2004; presented as Paper 2004-4897 at the AIAA Guidance, Navigation, and Control Conference, Providence, RI, 16–19 August 2004.

*Graduate Research Assistant, Aerospace Engineering Department/Space Systems Laboratory; currently Graduate Fellow, Department of Aeronautics and Astronautics, School of Engineering, Stanford University, Room 017, Durand Building, 496 Lomita Mall, Stanford, CA 94305-4035; dchavez@stanford.edu. Student Member AIAA.

†Assistant Professor, Aerospace Engineering Department/Space Systems Laboratory; atkins@eng.umd.edu. Senior Member AIAA.

architectures such as Object Agent have been developed to assist mission designers and operations personnel, providing a variety of visualization tools and interactive monitors to display real-time data from simulation or satellites.[12,13] Agent-based tools have been proposed for coordination and planning of formation activities to enable large satellite clusters to be effectively designed and managed without prohibitive personnel support.[14] Formation-flying testbeds have emerged as an important ground-based evaluation platform for verifying mission designs as well as navigation and control algorithms.[15]

For circular orbit formation mission design and analysis, the linearized Clohessy–Wiltshire equations are commonly used to find an elegant analytical solution when possible.[7,16] Researchers have also characterized the effects of gravitational perturbations, most notably the oblateness term J_2, and have developed equations useful for mission and controller design.[17–19] Extensions of analytic solutions to eccentric reference orbits have also been developed.[20]

Numerical optimization methods are required when analytical solutions are not available, as for the highly elliptical three-dimensional tetrahedron formation studied in this work. Genetic algorithms have been applied to identify desirable formation orbits and assembly maneuvers with complex cost functions that include terms such as path length, fuel consumption, relative fuel distribution, and collision penalties.[21] A host of other optimization algorithms have been adapted to formation mission design, including mixed-integer linear programming[22] and optimal control[23] algorithms applied to formation assembly problems. Jilla and Miller[24] have evaluated a variety of optimization techniques applied to the design of distributed spacecraft architectures and have identified a heuristic simulated annealing algorithm as the most promising approach. Other researchers[25,26] have studied large formations classified as "swarms," working to reduce the design space and maximize parallelization in the design effort given the large parameter space to be examined. This research adopts a hierarchical optimization algorithm that enables top-down identification of the optimal result with minimal overhead and employs a Lambert algorithm[27] for virtual rigid body (VRB) and dual-impulse formation designs, variants of which have more frequently been applied to assembly problems.[28]

Once formation requirements are specified and missions are designed, onboard systems must enable precise maintenance of formation geometries despite disturbances or adverse gravity fields. Relative navigation and control algorithms have been specifically developed for spacecraft formation flight.[29–32] Such techniques have been studied for natural-orbit and active control missions and frequently are needed to achieve extremely high-precision results.

The concept of a virtual structure,[32] virtual satellite,[14] or VRB[33,34] has been developed to facilitate formation specification and management, particularly when high-precision geometries must be maintained. With such a representation, each spacecraft acts as a node in an overall formation structure held together by natural and active control forces rather than by rigid physical components.

This work relies on a VRB representation to construct an actively controlled tetrahedron mission design that maintains a precise regular tetrahedron over extended time periods despite a countering central force. The goals of this research are to develop natural and actively controlled VRB mission designs for a tetrahedron geometry applicable to the proposed MMS mission and to comparatively evaluate these designs based on fuel consumption and potential scientific return. Emphasis is placed on problem formulation and characterization of optimal results for natural-orbit and VRB solutions, as well as a more practical dual-impulse solution derived from the VRB formulation. The VRB representation is defined and assumptions are discussed. To combat the significant computational complexity faced during formation mission design, an efficient hierarchical optimization algorithm is described that identifies an optimal solution despite a reduced search space. By assuming a regular tetrahedron of the desired size at apogee for this comparative analysis, the natural-orbit design vector over all satellites is simplified to a group of four unified parameters, significantly reducing optimization computational complexity. For the VRB case, exhaustive search and hierarchical optimization results are compared for a mission design with one active control region over which geometry is precisely maintained around apogee. VRB and natural-orbit designs are compared, followed by a dual-impulse solution that emulates the VRB but does not require active thruster use during data collection. A brief conclusion summarizes results and outlines future work required to identify a finalized tetrahedron mission design.

Virtual Rigid Body Definition

To describe the motion and geometry of each VRB formation, we define a series of reference coordinate frames.[33,34] First, inertial frame I is situated at the center of mass of the central body. Next, target frame T is defined as a reference to be tracked by the entire formation. The T-frame is assigned a natural orbit and therefore has associated orbital elements a, e, i, Ω, ω, and ν (Ref. 35). The orbital elements of T define a baseline formation translation for the VRB with respect to the central body. All coordinate frame rotational motions can be specified with an inertial or Earth-pointing reference. A formation "vehicle" frame V defines a rigid body offset and orientation of the entire formation with respect to T. Initially, V-frame location is typically defined either at the formation centroid or at one of the satellites. Each satellite k of the formation has an attached frame D_k that specifies its position and orientation relative to the V-frame. Figure 1 illustrates the frame set used to uniquely define VRB spacecraft formations. Natural-orbit formations will typically require unique orbital elements for each spacecraft, but an analysis such as that described in this paper can reduce the overall optimization vector to a manageable size.

In the case of the nonpermanent VRB design employed in this research, a region exists where the satellites actively maintain their relative positions, with the satellites freely drifting outside this region. The active control region has angular width λ and is situated

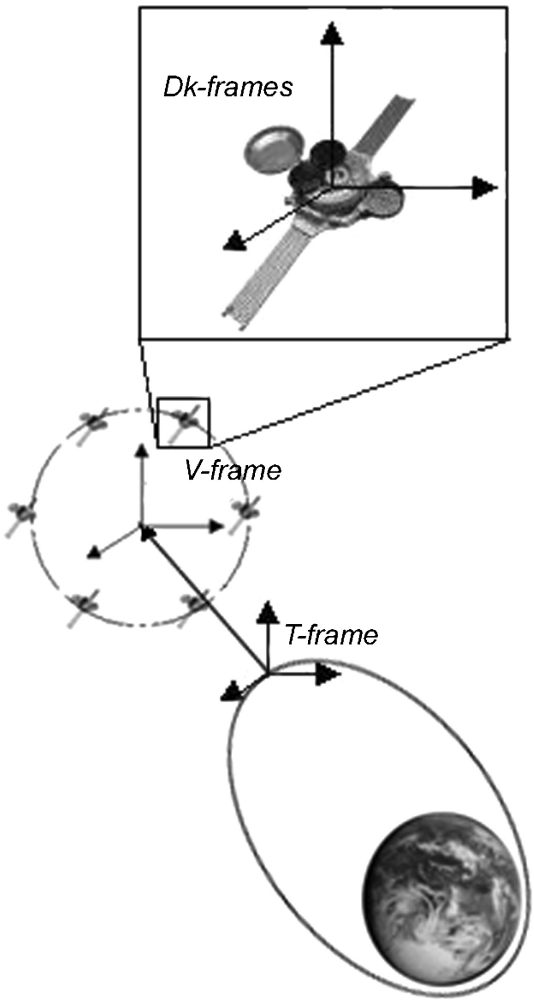

Fig. 1 Reference frames for VRB satellite formations.

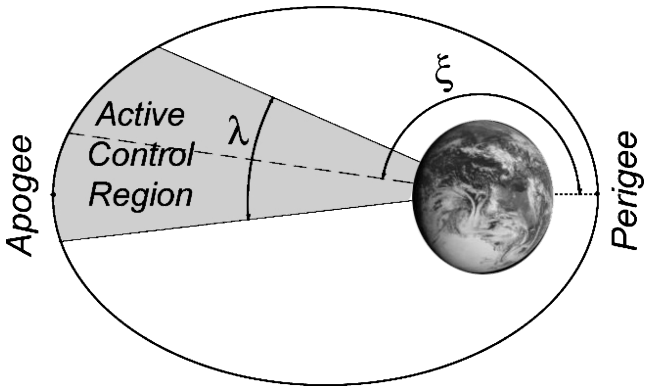

Fig. 2 Location and width of active control region for an elliptical orbit.

by ξ, the angle from perigee to the center of the active control region measured in the direction of orbital motion, as shown in Fig. 2.

Assumptions

This work makes several assumptions to enable use of standard astrodynamic analytical models and algorithms during optimization processes:

1) Satellites are subject to Keplerian dynamics only. Perturbations will change numerical results but not fundamental properties of natural-orbit or VRB solutions, especially for high-altitude orbits at high inclinations where the effect of perturbations is mitigated. Although the exact optimal solution will differ with perturbations, the general trends of the solution will not vary significantly.

2) Instantaneous ΔV is possible, enabling use of Lambert's solution for the VRB and dual-impulse mission designs.

3) Thrust is possible in any direction at any time without the need for reorientation.

4) The formation repeats every orbit and is presumed to be long-term. Assembly costs are ignored, and optimization is performed over one maintenance orbit with equal initial and final states.

5) Any orbital station at which the tetrahedron is sufficiently regular, as measured by the corresponding quality factor, is presumed to enable scientific data collection. Realistically, the observation region is limited, with useful measurements possible only during passage through the magnetopause.[36]

A significant body of research has been done to model orbit perturbations, and it would be feasible to extend the models and algorithms in this research to include the J_2 term. However, the primary goal of this research is to compare fundamentally different formation design strategies for an Earth-orbiting tetrahedron formation, a task for which Keplerian problem formulations significantly simplify understanding of optimal solution characteristics as well as minimizing optimization computational complexity. This work will enable relatively rapid prototyping of very different mission designs as a first step to selecting the "class" of mission design (natural, VRB, or dual- or multiimpulse). For any mission, once the mission design class is selected, additional analysis is inevitably required to more precisely identify optimal formation parameters with a high-fidelity dynamics propagator that captures J_2 and other perturbation terms potentially of similar significance for a highly eccentric reference orbit such as that proposed for MMS.

Work is under way to take these perturbations into account and characterize their impact on the overall cost of the missions here studied. Ultimately, our goal is to merge the hierarchical optimization tool with a high-fidelity propagator developed as part of our VRB simulation testbed, which accounts for gravity harmonics including J_2, solar radiation pressure, atmospheric drag, and third-body perturbations due to the moon and planets.[37]

Hierarchical Optimization Algorithm

Figure 3 shows the hierarchical algorithm used to optimize the parameters $\tilde{X} = [x_1 \;\; x_2 \;\; \ldots \;\; x_N]$ for natural and VRB formations. In this formulation, each design variable x_i has range $[x_i^{\min}, x_i^{\max}]$,

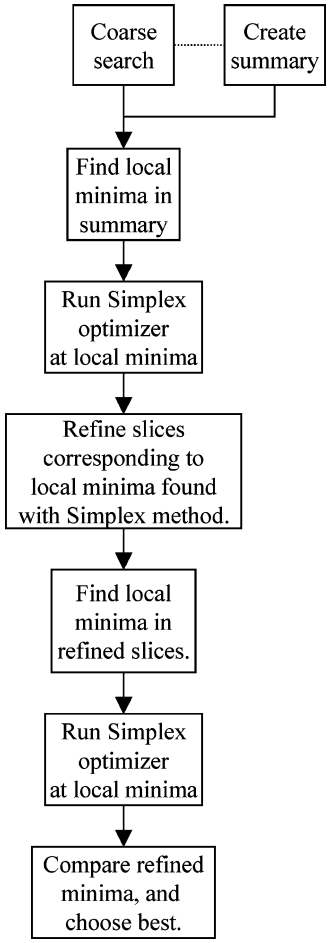

Fig. 3 Block diagram of hierarchical optimization.

and no constraints are imposed. The optimization steps are outlined next:

1) *Perform a coarse exhaustive search.* To identify an initial set of local minimum regions, an exhaustive search is performed over all design vector combinations given step sizes $\Delta\tilde{X} = [\Delta x_1 \;\; \Delta x_2 \;\; \ldots \;\; \Delta x_N]$, which yields

$$nx_i = \text{floor}\left(\frac{x_i^{\max} - x_i^{\min}}{\Delta x_i}\right) + 1$$

points for each x_i. Given limited knowledge of cost variation as a function of design parameters, one can construct this search grid to maximize the likelihood of converging to a globally optimal final result. For the formation flying architectures presented in this paper, previous work provides sufficient understanding of the search-space behavior so that the grid can be selected to guarantee the identification of the global optimum.[36]

2) *Identify local minima from coarse search.* An optimal cost for each of the nx_i values of x_i is computed as the minimum cost value over all other $(n-1)$ coarse search variable value combinations. A summary table $\boldsymbol{S}$ is constructed as $\tilde{S}_{ij} = [(x_1)_{ij} \;\; (x_2)_{ij} \;\; \ldots \;\; (x_N)_{ij}]$ vectors describing each local minimum j found over the optimal-cost plots for each x_i.

3) *Utilize local optimization series to refine local minima.* The goal of coarse search was to identify local minimum regions but not exact solutions. In this step, an exact local minimum for each summary table entry $\tilde{S}_{ij}$ is computed. Numerous unconstrained methods could be applied; the Simplex method of Nelder and Mead was chosen due to its availability within the GNU Scientific Library (GSL) (available at http://sources.redhat.com/gsl/) and its widespread use. Note that all optimization code was implemented in C, and GSL acted as a C "toolbox" for existing vector/matrix math functions. Nelder–Mead is a method of order zero that does not require knowledge of gradient information.

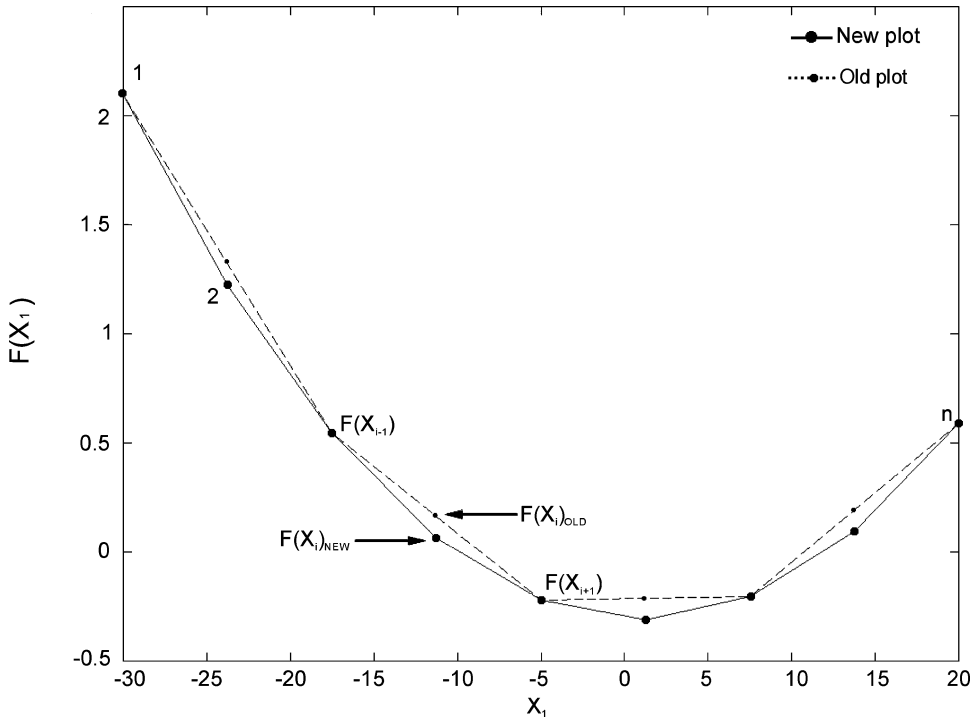

Fig. 4 Consecutive steps of the refinement process.

4) *Iteratively refine solution.* A refinement is performed to improve the characterization of cost as a function of each design variable. This refinement can also identify new local minimum regions in cases where the initial search was too coarse. For each updated local minimum $\tilde{S}_{ij}$ of each x_i from step 3, x_i vs cost [or generally $F(x_i)$] is stored for each of the nx_i initial grid points, assigning the other $(n-1)$ design variables their $\tilde{S}_{ij}$ values. A simple quadratic function example is shown in Fig. 4 for an x_1 ranging from -30 to 20 with $(nx_1 = 5,\ \Delta x_1 = 12.5)$. A series of new intermediate cost values $F(x_i)_{\text{NEW}}$ are computed as shown. The new doubled set of x_i values is iteratively refined until the mean percent error (MPE) drops below a user-specified error threshold ε:

$$\left(\text{MPE} = \frac{1}{n_{\text{new}}}\sum_{i=1}^{n_{\text{new}}}\left|\frac{F(x_i)_{\text{NEW}} - F(x_i)_{\text{OLD}}}{F(x_i)_{\text{OLD}}}\right|\right) \le \varepsilon \qquad (1)$$

where n_{new} is the number of points recalculated and $F(x_i)_{\text{OLD}}$ is the average of the previous and subsequent design vector values:

$$F(\tilde{X}_i)_{\text{OLD}} = F(\tilde{X}_{i-1}) + F(\tilde{X}_{i+1})/2 \qquad (2)$$

5) *Find local minima in refined plots and perform local optimizations.* The result of step 4 is a list of search-space slices sampled in detail. Each slice consists of a set of objective function samples obtained with all variables held constant except x_i and is akin to investigating the sensitivity of the objective function with respect to x_i. This step updates the summary table $\boldsymbol{S}$ with the iterative refinement results. The procedure from steps 2 and 3 is repeated for all refined slices to obtain new global minimum candidates.

6) *Identify optimal result.* As a final step, the optimal (i.e., minimum-cost) entry $\tilde{S}_{ij}$ is identified from the updated $\boldsymbol{S}$ and saved as the final solution.

Natural Orbit Tetrahedron Optimization

Hierarchical optimization was applied to a tetrahedron satellite formation constrained to naturally assemble at apogee. This geometry is motivated by the European Space Agency's Cluster II and NASA's proposed magnetospheric multiscale (MMS) mission. The natural-orbit optimization goal is to find the best orbital elements for all formation satellites. Below, a review of tetrahedron quality factors is provided, followed by a derivation of a minimally complex design vector. The optimization results are then presented and analyzed.

Tetrahedron Geometric Quality Factors

A suite of quality factors were developed for the Cluster II mission that apply to any general tetrahedral formation such as MMS.[38] The Glassmeier and Robert–Roux parameters were chosen for Cluster II because of their geometric insight.[39] The Glassmeier parameter Q_G was proposed in 1992 by vom Stein, Glassmeier, and Dunlop (see Ref. 39). It takes values [1 3] and describes the dimensionality of the tetrahedron, with $Q_G = 1.0$ indicating that all spacecraft are colinear, $Q_G = 2.0$ the case when all spacecraft lie in a plane, and $Q_G = 3.0$ a regular tetrahedron:

$$Q_G = \frac{\text{true volume}}{\text{ideal volume}} + \frac{\text{true surface}}{\text{ideal surface}} + 1 \qquad (3)$$

In Eq. (3), ideal values are the total volume and surface of a regular tetrahedron with side lengths equal to the average of the six distances between the four spacecraft, and the true values are the actual inter-spacecraft distances computed at a particular time (snapshot). The Robert–Roux parameter Q_R was proposed in 1993 to measure the regularity of a tetrahedron and has values

$$Q_R = N \cdot \left(\frac{\text{true volume}}{\text{sphere volume}}\right)^{\frac{1}{3}} \qquad (4)$$

"Sphere volume" from Eq. (4) is derived from a sphere that circumscribes the tetrahedron with all four satellites on its surface. The factor N is a normalization factor that adjusts the range of Q_R to fall in the range [0 1]. If the spacecraft are coplanar or colinear, the circumscribing sphere is either undefined or not uniquely defined and then Q_R is undefined. In this work, the spacecraft were never exactly coplanar or collinear; only Q_R was utilized. It should be noted that the quality factors are a measure exclusively of how well actual formation shape matches a regular tetrahedron, but they provide no information about size or spatial orientation.

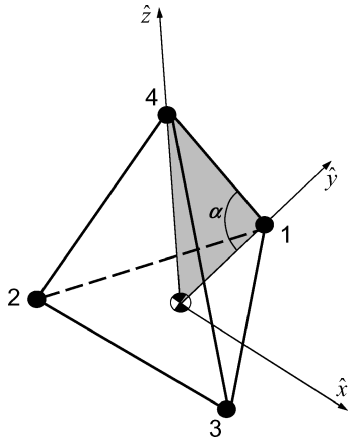

Fig. 5 Regular tetrahedron illustrating *V* frame and internal angle α.

Optimization

To optimize the natural-orbit tetrahedron formation, two simplifying assumptions were made. First, the tetrahedron is presumed to be regular ($Q_R = 1$) when all satellites are at apogee. This assumption, although not fully general, yields extended high-quality observation periods and facilitates comparison with VRB solutions that require minimum fuel when centered about apogee. Next, the tetrahedron is designed to synchronously assemble after every orbit, so all satellite orbital periods and thus semimajor axes a must be equal.

A minimal set of optimization parameters are identified that meet the constraints associated with these two assumptions, both of which require a fixed reference point for apogee. Recall that for the VRB, target reference T and "vehicle" V frames are defined. For all VRB and natural-orbit analyses, V is affixed to the formation as shown in Fig. 5 with origin located at the centroid of the base, V_y directed toward satellite 1, V_z pointing toward satellite 4, and V_x completing the right-handed reference frame. Note that T-frame inclination does not affect cost because strictly Keplerian dynamics are presumed.

For the VRB, the T frame is followed throughout the orbit. However, for our natural-orbit solution, each satellite follows a separate orbit but with identical periods/semimajor axes, yielding a total of five target frames (T, T_1, T_2, T_3, T_4), where T_i is the reference target frame for each satellite i from Fig. 5, and T is the single-formation reference frame:

$$P = 2\pi\sqrt{a^3/\mu} \tag{5}$$

To determine the optimal orbital parameters for each T_i, a minimal design vector is developed to constrain the system to form a regular tetrahedron at apogee. This restricted solution is designed to construct an intuitive design vector complete over orbital elements but without the ability to optimize over different (nonapogee) assembly stations v or tetrahedron orientations q relative to the inertial frame. Given semimajor axis a, the remaining orbital elements are geometrically constrained. The eccentricity of a satellite, e, is defined by its required apogee radius:

$$r_{a,i} = a(1 + e_i) \tag{6}$$

$$e_i = (r_{a,i}/a) - 1 \tag{7}$$

The orientation of the orbit in space must now be chosen so that when the satellite reaches apogee, it will be at the position dictated by the reference T-frame coordinates. This condition can be satisfied by aligning the line of apsides with the desired radius vector of the satellite. In terms of the eccentricity vector, this may be expressed as

$$\hat{e} = -\hat{r}_{\text{sat}} \tag{8}$$

where $\hat{\boldsymbol{e}} = \boldsymbol{e}/e$ and $\hat{\boldsymbol{r}}_{\text{sat}} = \boldsymbol{r}_{\text{sat}}/r_{\text{sat}}$ are unit vectors.

A family of orbits satisfy this condition. Specifically, if the eccentricity vector is aligned as indicated, the orbit can be freely rotated about $\hat{e}$ and still satisfy the apogee location. Such a rotation (ρ) affects orbital elements i, Ω, and ω and is the equivalent of rotating the angular momentum vector $\boldsymbol{h}$ about $\hat{\boldsymbol{e}}$. This last degree of freedom must be constrained by choosing consistent values for i, Ω, and ω; then any combination of four such orbits will generate the proper apogee geometry. We first identify one $\boldsymbol{h}$ that satisfies the desired apogee conditions; then all its rotations about $\hat{\boldsymbol{e}}$ also satisfy the constraints. One such orbit has line of nodes perpendicular to the line of apsides, assuming an inclined orbit. In this case, inclination is the complement of the angle between $\hat{\boldsymbol{e}}$ and the Z axis:

$$i = 90\,\text{deg} - \cos^{-1}(\hat{\boldsymbol{e}} \cdot \boldsymbol{Z}) \tag{9}$$

If $i > 0$ deg, the longitude of the ascending node is equal to 90 deg plus the angle between the projection of $\hat{\boldsymbol{r}}_{\text{sat}}$ onto the X–Y plane and the X axis:

$$\hat{\boldsymbol{r}}_{\text{proj}} = [\hat{r}_X \quad \hat{r}_Y \quad 0] \tag{10}$$

$$\Omega = 90\,\text{deg} + \cos^{-1}(\hat{\boldsymbol{r}}_{\text{proj}} \cdot \boldsymbol{X}) \tag{11}$$

Note that the argument of perigee for this case satisfies

$$\omega = 90\,\text{deg} \tag{12}$$

If $i = 0$ deg, Ω is undefined, and ω is replaced by the longitude of perigee (ϖ), now satisfying

$$\Omega = 0\,\text{deg} \tag{13}$$

$$\varpi = \sin^{-1}(\boldsymbol{X} \times \hat{\boldsymbol{e}})$$

$$\text{if} \qquad (\boldsymbol{X} \times \hat{\boldsymbol{e}})_Z < 1, \qquad \varpi = 2\pi - \varpi \tag{14}$$

Finally, if inclination $i < 0$ deg, perigee is below the equatorial plane, and we can simply use the absolute value of inclination, calculating the remaining orbital elements as follows:

$$i = |i|, \qquad \omega = -90\,\text{deg}, \qquad \Omega = \cos^{-1}(\hat{\boldsymbol{r}}_{\text{proj}} \cdot \boldsymbol{X}) - 90\,\text{deg} \tag{15}$$

All orbital elements are now defined, and a standard procedure is used to find $\boldsymbol{r}$ and $\boldsymbol{v}$.[39,40] The angular momentum vector $\boldsymbol{h} = \boldsymbol{r} \times \boldsymbol{v}$ can then be computed.

To identify the family of orbits that result from rotating $\boldsymbol{h}$ about $\hat{\boldsymbol{e}}$, Rodrigues's formula was applied to define the rotation of a vector $\boldsymbol{Q}$ about a unit vector $\hat{\boldsymbol{k}}$:

$$\boldsymbol{Q}' = \boldsymbol{Q}\cos\theta + \sin\theta(\hat{\boldsymbol{k}} \times \boldsymbol{Q}) + (1 - \cos\theta)(\hat{\boldsymbol{k}} \cdot \boldsymbol{Q})\hat{\boldsymbol{k}} \tag{16}$$

Substituting $\boldsymbol{Q} = \boldsymbol{h}$, $\hat{\boldsymbol{k}} = \hat{\boldsymbol{e}}$, and $\theta = \rho$, this equation becomes

$$\boldsymbol{h}' = \boldsymbol{h}\cos\rho + \sin\rho(\hat{\boldsymbol{e}} \times \boldsymbol{h}) + (1 - \cos\rho)(\hat{\boldsymbol{e}} \cdot \hat{\boldsymbol{h}})\hat{\boldsymbol{e}} \tag{17}$$

where ρ is the rotation angle about $\hat{\boldsymbol{e}}$ measured from the reference position from Eqs. (10–16). This rotation does not change a or e. The remaining orbital elements are

$$i = \cos^{-1}(h'_Z/h') \tag{18}$$

$$\Omega = \cos^{-1}(n_X/n), \qquad \text{where} \qquad \boldsymbol{n} = \hat{\boldsymbol{Z}} \times \boldsymbol{h}'$$

$$\text{if} \qquad n_Y > 0, \qquad \Omega = 360\,\text{deg} - \Omega \tag{19}$$

$$\omega = \cos^{-1}(\boldsymbol{n} \cdot \boldsymbol{e}/ne), \quad \text{if} \qquad \hat{\boldsymbol{e}}_Z > 0, \qquad \omega = 360\,\text{deg} - \omega \tag{20}$$

$$\nu = 180\ \text{deg (apogee)} \tag{21}$$

The optimization search space now consists of only four parameters: spacecraft orbit orientations ρ_1, ρ_2, ρ_3, ρ_4. To select an optimal set of orientations, a cost function J is defined with three

parts: an "integrated" Q_R term, an "integrated" Q_G term, and a fuel-consumption term

$$J = w_1\left(\sum_{Q_{R,i} \geq Q_{R,\min}} Q_{R,i} \cdot \Delta t\right) + w_2\left(\sum_{Q_{G,i} \geq Q_{G,\min}} Q_{G,i} \cdot \Delta t\right) + w_3\left(\frac{\Delta V_{\text{Total}}}{T_{\text{obs}}}\right) \tag{22}$$

where w_1, w_2, w_3 are weighting factors, $Q_{R,\min}, Q_{G,\min}$ are minimum acceptable values of Q_R and Q_G, $Q_{R,i}$, $Q_{G,i}$ are Q_R and Q_G at station i in the orbit, Δt is the orbit-propagation time step, ΔV_{Total} is the total ΔV applied around the orbit, and T_{obs} is the time of observation per orbit. For the natural-orbit results described below, $w_1 = -1$ and $w_2 = w_3 = 0$, defining Q_R as utility. Note that w_1 is negative because quality factor is maximized.

Natural Orbit Results

The MMS mission will have tetrahedron edge lengths (intersatellite distances) ranging from 10 to 10,000 km. The 10-km case is optimized first, and T-frame orbital elements are initialized to ($a = 61{,}230.144$ km, $e = 0.875$, $i = 0.0$ deg, $\Omega = 0.0$ deg, $\omega = 0.0$ deg), candidate values for MMS.[6] Optimization of (ρ_1, ρ_2, ρ_3, ρ_4) was performed with quality-factor threshold $Q_{R,\min} = 0.70$. The optimal result has $\rho_1 = \rho_2 = \rho_3 = \rho_4 = 5.32761754$ rad $= 305.25$ deg, with further details provided in Table 1. This is an intuitive solution because if all orbit rotation angles are the same, the spacecraft will be moving roughly in the same direction at apogee (i.e., their velocity vectors will be nearly parallel). The rate of change of relative velocity is also lower in this case than when one or more of the satellites have different orbit orientations. To better understand why $\rho_{\text{opt}} = 305.25$ deg is optimal, consider the internal angle α of a regular tetrahedron (see Fig. 5), formed between the line joining satellites 1 and 4 and the plane formed by the base of the tetrahedron (satellites 1–3). For a regular tetrahedron, $\alpha = 54.75$ deg. Given that the rotations ρ are about $\hat{\boldsymbol{e}}$, which points toward perigee, the angle β between the satellite orbital planes and the equatorial plane is

$$\beta = 360\,\text{deg} - \rho_{\text{opt}} = 54.75\,\text{deg} \tag{23}$$

Angles α and β are the same, indicating that in the optimal solution the satellite orbital planes are parallel to the 1–4 line. This suggests there might indeed be two solutions, one with a posigrade and one with a retrograde orbit, provided that both are parallel to the 1–4 line. Consider the behavior of

$$J = \sum_{Q_{R,i} \geq Q_{R,\min}} Q_{R,i} \cdot \mathrm{d}t$$

as ρ changes, assuming $\rho_1 = \rho_2 = \rho_3 = \rho_4 = \rho$. Figure 6 shows this trend, and verifies the existence of two maximum-utility solutions at $\rho = 5.327618$ rad (305.25 deg) and $\rho = 2.186025$ rad (125.25 deg). The second solution is, in fact, a retrograde orbit set. Notice that the application of the retrograde solution in actual mission design might be limited because of the higher velocity increment required to launch a satellite into a retrograde orbit. Figure 6 also shows that there are two minimum-utility rotations at $\rho = 0.615229$ rad (35.25 deg) and $\rho = 3.756822$ rad (215.25 deg). At these angles, the orbital planes are perpendicular to the line joining satellites 1 and 4.

Figure 7 shows the variation of the Robert–Roux parameter (Q_R) throughout a complete orbit for the highest- and lowest-utility cases with equal orbit rotations for all four spacecraft. The curve starts at perigee ($t = 0$), where Q_R is low. The maximum is at apogee, an expected result given that the regular tetrahedron is assembled precisely. The shaded areas illustrate the integrated Q_R region, included in total cost (utility), because quality is above the 0.7 threshold. Figure 8 illustrates Q_R over one orbit for several equal-ρ cases. As shown, no two curves intersect except at apogee. Because the optimal $\rho = 5.327618$ rad has maximum Q_R throughout the orbit, this solution has the highest utility regardless of threshold $Q_{R,\min}$.

Next consider why the solution with all satellites having equal $\rho = 305.25$ deg yields the maximum integrated utility. Due to geometry, the angular separation between the satellite orbital planes is a function of orbit rotation angles. The regular tetrahedral shape is maintained over a larger portion of the orbit, with small angular separations, because the satellite motions are closest to being coplanar. This intuition is confirmed in Fig. 9, showing the maximum angular separation between orbital planes as a function of ρ. The plot is obtained by finding the maximum angle between any pair of formation satellite $\boldsymbol{h}$ vectors for each value of ρ shown. Maximum and minimum angular separations coincide with the lowest- and highest-utility solutions, respectively. Note that the piecewise construction results from different satellite pairs contributing the largest separation, as indicated near the bottom of Fig. 9 with satellite numbering from Fig. 5.

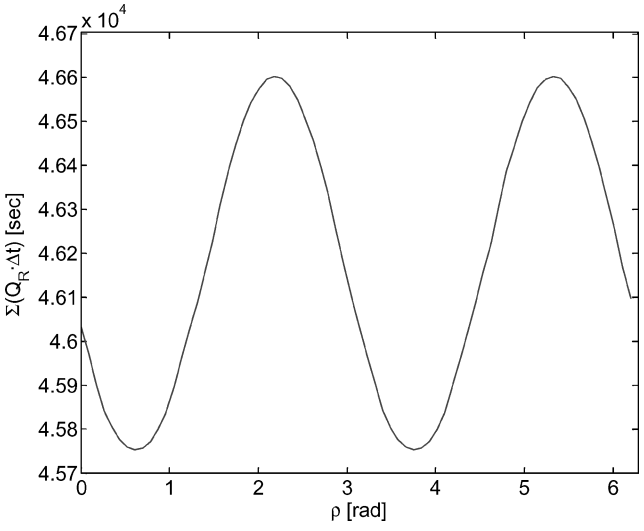

Fig. 6 Utility ($Q_R * \mathrm{d}t$) vs rotation angle (large utility = better solution).

Table 1 Optimal solution for the natural-orbit tetrahedron

Parameter	Solution
$J = \sum_{Q_{R,i} \geq Q_{R,\min}} Q_{R,i} \cdot \mathrm{d}t$	4.660182×10^4 s
t_0	49,457.5692 s (from perigee)
t_f	101,346.5511 s (from perigee)
$T_{\text{obs}} = t_f - t_0$	14.4136 h (34.41% of the orbit)
	Orbital elements (a, km; e, i, rad; Ω, rad; ω, rad)
Satellite 1	{61,230.144, 0.875000, 0.95556776548, 3.1415423951, 3.1415926536}
Satellite 2	{61,230.144, 0.875082, 0.95556776548, 3.1416178253, 3.1415926536}
Satellite 3	{61,230.144, 0.874918, 0.95556776548, 3.1416178275, 3.1415926536}
Satellite 4	{61,230.144, 0.875000, 0.95556776727, 3.1415423604, 3.1416797949}

Table 2 Optimal solutions for different tetrahedron sizes

Separation, km	ρ_1, rad	ρ_2, rad	ρ_3, rad	ρ_4, rad	Utility, s	T_{obs} h
10	5.327618	5.327618	5.327618	5.327618	4.660182×10^4	14.4136 (34.41%)
100	5.255800	5.255800	5.255856	5.255800	4.659759×10^4	14.4136 (34.41%)
1,000	5.257592	5.257593	5.257592	5.256974	4.656325×10^4	14.4031 (34.38%)
5,000	5.256960	5.266099	5.266478	5.273388	4.624935×10^4	14.3089 (34.16%)
10,000	0.504899	4.873276	4.762386	2.765658	5.120226×10^4	2.6754 (6.39%)

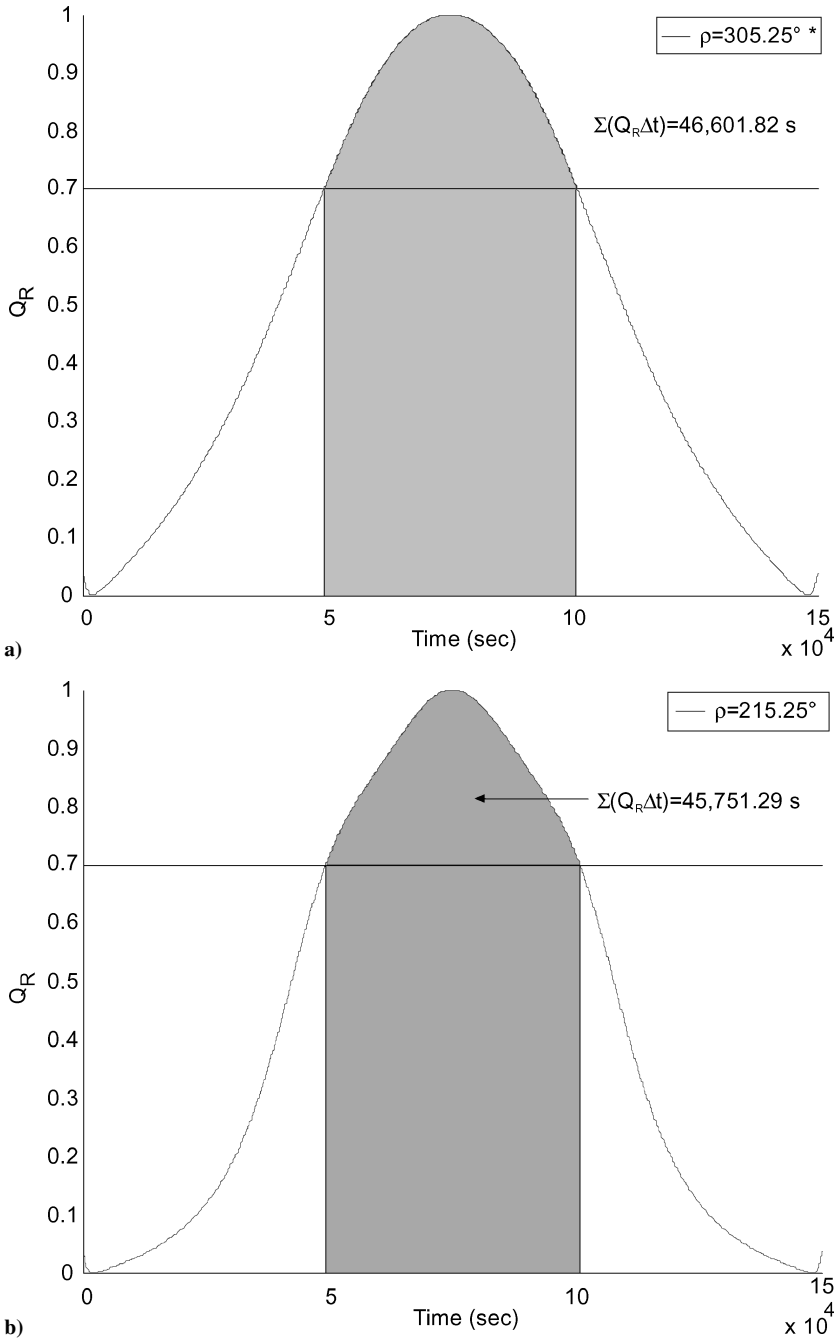

Fig. 7 Variation of Q_R throughout the orbit for the a) best and b) worst configuration from Fig. 6.

To verify whether the optimal rotation-angle solution is general beyond the 10-km satellite separation distance, optimization was performed for four more cases, with separations of 100, 1000, 5000, and 10,000 km. Results are summarized in Table 2 and indicate that the 10-km solution is not a general result. For 100-, 1000-, and 5000-km separations, optimal angles ρ are very close to those for the 10-km case. However, the 10,000 km tetrahedron has a significantly different optimal solution with different ρ. This is likely because the semimajor axis a is of the same order of magnitude as the satellite separations. Note that T_{obs} with $Q_R \geq 0.7$ decreases as the separation increases. Note also that the Cluster II mission, currently in flight, uses an approach similar to our natural-orbit solution, with the tetrahedron naturally assembled at apogee without fuel expenditure. Propellants are used to initially assemble or reconfigure the formation (e.g., change tetrahedron size), the full optimization of which is beyond the scope of this paper.

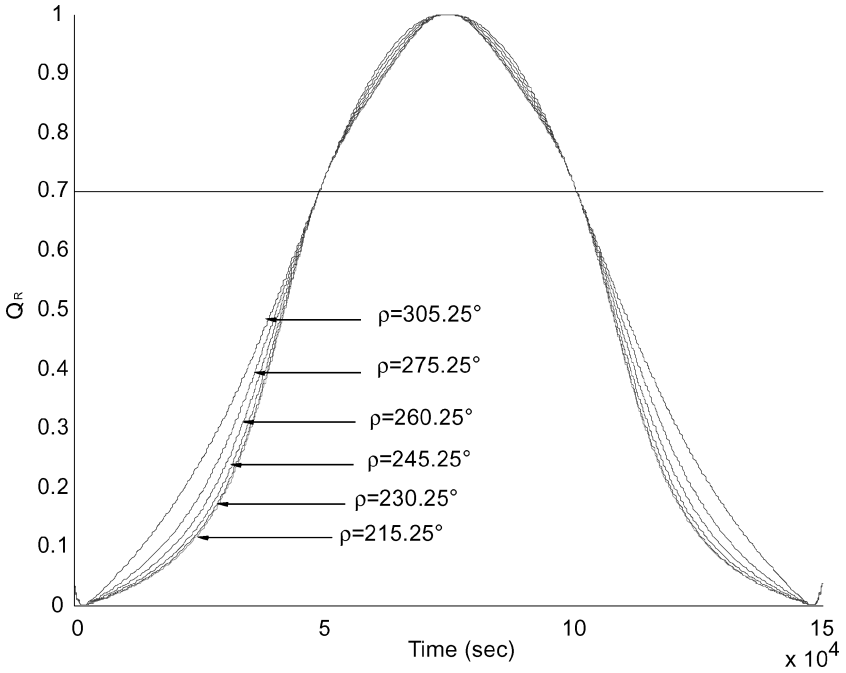

Fig. 8 Q_R variation for rotations between best and worst 10-km solutions.

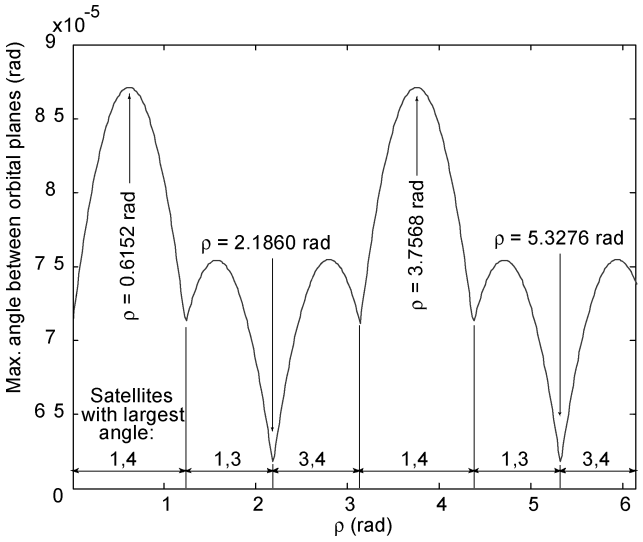

Fig. 9 Angular separation between orbital planes at different orbit rotation angles.

Virtual Rigid Body Case

Consider now the case in which fuel is expended to actively maintain the MMS regular tetrahedron as a VRB. Recall that our VRB formulation requires definition of target frame T orbital elements, a vector V (presumed constant) describing VRB offset from T, and an active control region (λ, ξ) over which the VRB is actively maintained. At the active control region boundaries, impulsive maneuvers based on a Lambert solution are executed to reassemble the formation for the next active control pass.

Given our assumption of perfect Keplerian motion, an equatorial reference orbit T was presumed, because inclination will not affect cost, so that $\Omega = 0, i = 0$. T-frame a and e may also be fixed because their maximum values minimize fuel expenditure, and with fuel as the cost function, an active control region centered on apogee ($\xi = \pi$) is optimal.[33,34] T-frame a and e were set to 61,230.1 km and 0.875, respectively, as was the case for natural-orbit analyses. The VRB design vector is then (λ, ω, V_x, V_y, V_z), and results are presented for both exhaustive search and hierarchical optimization procedures.

Table 3 Summary of VRB results with one active control region per orbit

Parameter	Exhaustive search	Hierarchical opt.
λ	0.430 rad (24.64 deg)	0.427348 rad (24.49 deg)
ξ	3.1416 rad (180 deg)	3.1416 rad (180 deg)
a	61230.144 km	61230.144 km
e	0.875	0.875
ω	0.60 rad (34.38 deg)	2.518037 rad (144.27 deg)
V_x	−1.0 km	−0.927891 km
V_y	0.0 km	0.037552 km
V_z	−2.5 km	−2.757052 km
Obs. time T_{obs}	18.86 h (45.02% of the orbit)	18.76 h (44.78% of the orbit)
ΔV/s	2.351179×10^{-05} m/s^2	2.350654×10^{-05} m/s^2
ΔV/orbit (all satellites)	1.596356 m/s	1.587538 m/s
Program execution time	342 min	2 min 43 s

To verify hierarchical optimization results, exhaustive search over a fine grid was performed on a Beowulf cluster. Search parameters (λ, ω, V_x, V_y, V_z) ranged from (0.01 rad, 0.0001 rad, −5 km, −6 km, −8.3 km) to (0.5 rad, 3.14159 rad, 5 km, 3 km, 0 km), with step sizes (0.01 rad, 0.2 rad, 0.5 km, 0.5 km, 0.1 km). Although, the problem was estimated to require roughly 10–13 days on a 2-GHz Pentium 4, eight Beowulf nodes with Dual Intel Xeon CPUs at 2.80 GHz required 342 min execution time, measured from search-space initialization until identification of the optimal solution. Minimum cost values, where cost is strictly defined as Δv per observation second, are shown as a function of each search parameter in Fig. 10. Note that observation time for the VRB is by default defined as active control region duration, effectively requiring a regular tetrahedron of the specified size for data collection ($Q_{R,\min} = 1.0$). Cost varies smoothly over λ, with a single minimum at 0.43. For argument of perigee ω, the shape of the optimal-cost plot is not smooth, indicating the need for either a refined grid (and more computation time) or the more efficient hierarchical search to identify the global minimum solution. V-frame offset plots indicate two local minima for V_x, one for V_y, and one for V_z. Exhaustive search results are summarized in Table 3.

The same VRB tetrahedron formation was optimized by using the hierarchical algorithm from Fig. 3. The coarse search parameters (λ, ω, V_x, V_y, V_z) were assigned the same minimum and maximum

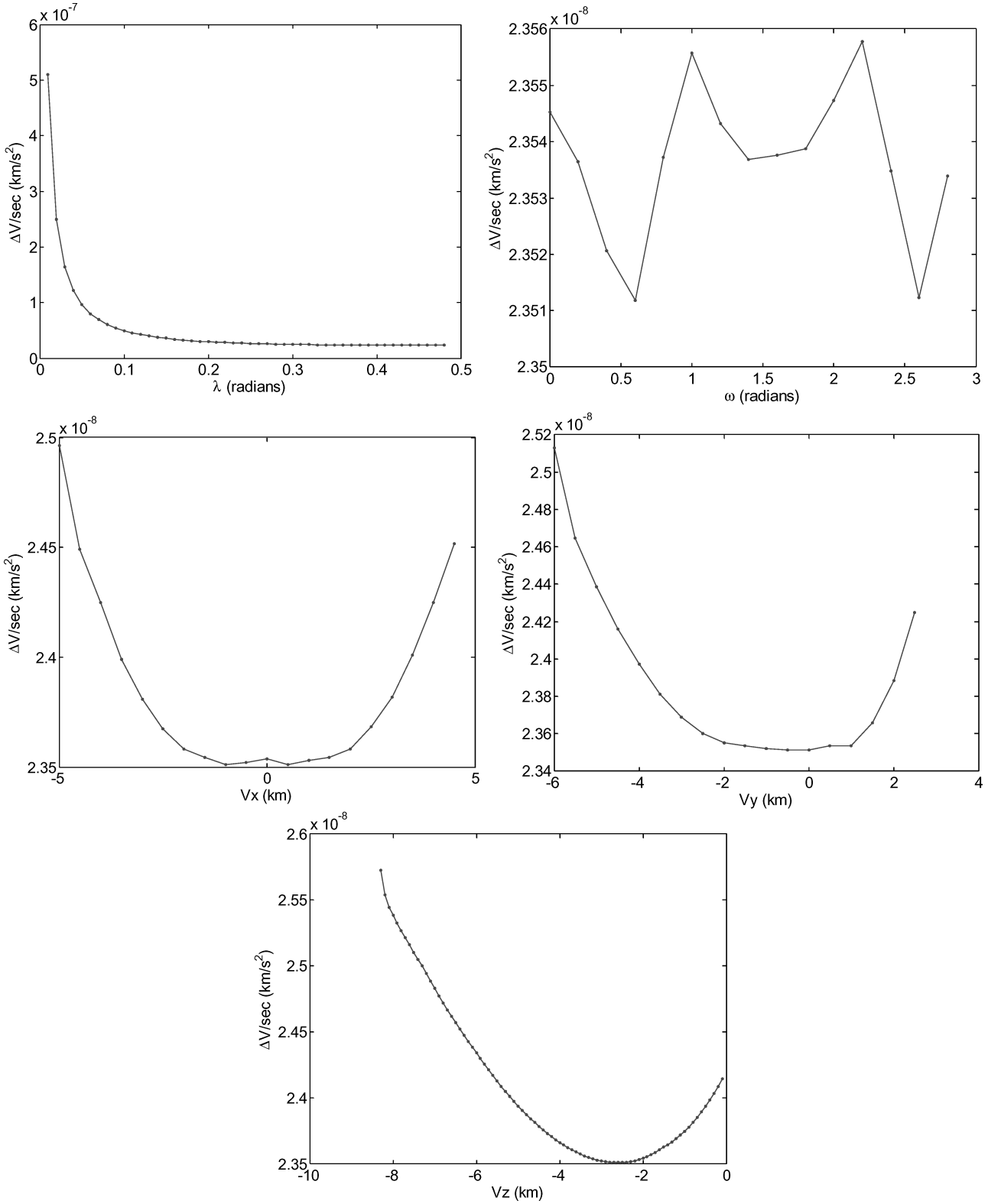

Fig. 10 Summary plots for the VRB formation from exhaustive search.

value sets as for exhaustive search but now with step sizes (0.2 rad, 0.25 rad, 2 km, 1 km, 1 km). The total number of sampled (coarse search) values is considerably smaller than that for the exhaustive search, and hierarchical search was easily executed on a single personal computer. A comparison of exhaustive and hierarchical optimization results is provided in Table 3. Although solutions were similar, except for ω, which converged to the two different minima illustrated in Fig. 10, the hierarchical method enabled identification of a solution with slightly higher utility (0.02%) than that obtained from exhaustive search in just under 3 min on a single 2-GHz Pentium 4 computer.

The VRB in this case was designed to center the active control region at apogee. Although the active region width λ is small, the VRB is still maintained for almost half the total orbital period. For a regular tetrahedron, the centroid has the same (X, Y) coordinates as the centroid of the base and is located at $\frac{1}{4}$ the height (Z). In

our case, the centroid coincides with the barycenter, given that all four spacecraft have equal masses. The optimal identified V-frame location (−0.9279, −0.0376, −2.7571) is close to the tetrahedron barycenter (0, 0, −2.0425).

Tradeoff Analysis

Thus far two different approaches to regular tetrahedron mission design have been presented: a natural-orbit solution constrained to assemble the tetrahedron at apogee, and an actively controlled solution in which a tetrahedron VRB was precisely maintained around apogee. Table 4 provides a comparison of the natural-orbit and VRB tetrahedron designs. Recall that in both cases cost (or utility) was calculated with Eq. (22), using the weighting factors discussed above. Also, note that cost calculations do not include the cost of assembling the formations, but instead are strictly the cost of maintaining the formation over each orbit. The optimal VRB provides 30% more observation time per orbit than the natural-orbit design even when observations are made only during active VRB maintenance. The VRB design also provides higher quality scientific data during this period because $Q_R = 1$. On the other hand, the natural-orbit design requires no propellant. A more consistent comparison is possible, however, by extending the VRB observation period into the drift region so that quality factor need not be perfect but must exceed threshold $Q_{R,\min} = 0.7$.

To explore the evolution of Q_R over both active and drift segments of the VRB mission design, quality factor Q_R was computed over one complete orbit and plotted in Fig. 11. Station (a) represents the beginning of active control and is designated as the initial state ($t = 0$). After 18.76 h, the active control region ends (station (b) in Fig. 11), and as the satellites drift, the quality factor decreases until it crosses below the threshold $Q_{R,\min} = 0.7$. During this drift segment, the tetrahedron is not perfect, but Q_R is sufficiently high to yield good scientific data. Q_R drops around perigee and then rises symmetrically until it crosses the 0.7 threshold. The result is that a considerably longer observation time is achieved naturally by the VRB design, as shown numerically in Table 4 for the VRB case, where $Q_R \geq 0.7$ rather than the perfect $Q_R = 1.0$.

The Table 4 summary makes a strong case for the VRB over the natural orbit design. First, scientific data can be collected for over 85% of the orbit, made possible with a combined $\Delta V = 1.588$ m/s per orbit (0.4 m/s per satellite). The average quality factor over the observation period is higher for the VRB, and the extended data collection time per orbit can yield more data over the mission, given that expected spacecraft component lifetime also factors into mission duration.

Dual-Impulse VRB Analog

Although attractive from a geometric perspective, the actively controlled VRB solution may be infeasible for MMS because particles output by thrusters may interfere with magnetic-field sensing equipment. Consider an alternative solution in which the regular tetrahedron is assembled precisely at two orbit stations, corresponding to the VRB active-drift transition stations in Fig. 2. With impulsive maneuvers applied at each of these stations, the VRB active-control region now becomes a second drift region, whereas the original VRB drift region is identical to its dual-impulse counterpart for a given (λ, ω, V_x, V_y, V_z). The applied impulse pair must reassemble the formation at the two specified stations and is computed for each satellite from a pair of Lambert's solution orbits, one per drift segment. This formulation enables reuse of the design vector (λ, ω, V_x, V_y, V_z), providing a close comparison with previous VRB results.

Table 4 Comparison between natural orbit, VRB, and dual-impulse designs

Parameter	Natural $Q_{R,\mathrm{MIN}} = 0.7$	VRB $Q_{R,\mathrm{MIN}} = 1.0$	VRB $Q_{R,\mathrm{MIN}} = 0.7$	Dual-impulse ($w_1 = 0$, $w_3 = 1$)
Time of observation per orbit, h	14.41	18.76	35.83	35.83
Observation % of total orbit period	34.41	44.78	85.51	85.51
ΔV/s (total over all satellites), m/s^2	0	2.350654×10^{-05}	1.230764×10^{-05}	6.2530×10^{-06}
ΔV/orbit (per satellite), m/s	0	0.4	0.4	0.2
Average individual satellite fuel mass per orbit (1000 kg mass, $I_{\mathrm{sp}} = 200$ s), kg	0	0.204	0.204	0.103
Average Q_R during observations	0.8827	1.0	0.9658	0.9501

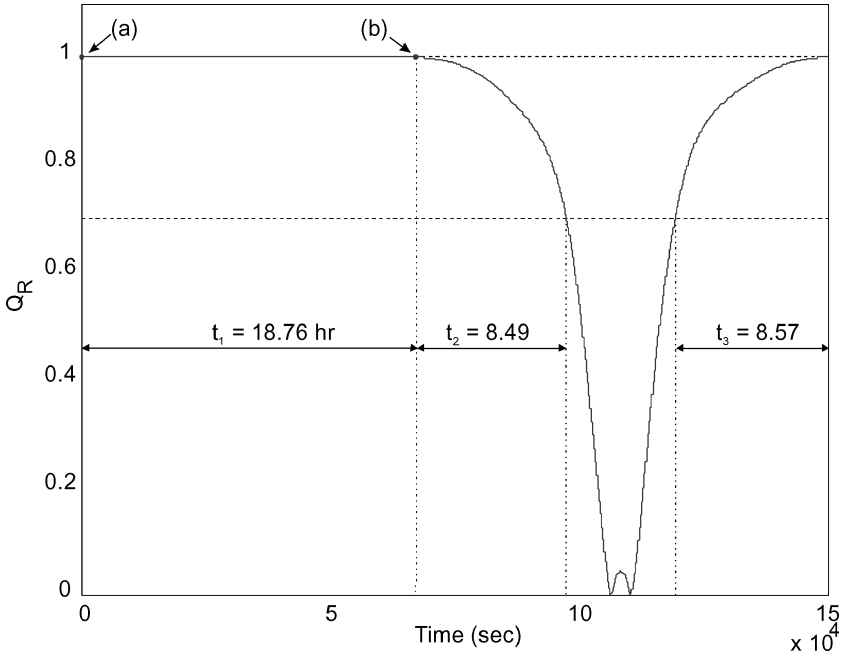

Fig. 11 Variation of Q_R throughout an entire orbit with the VRB design.

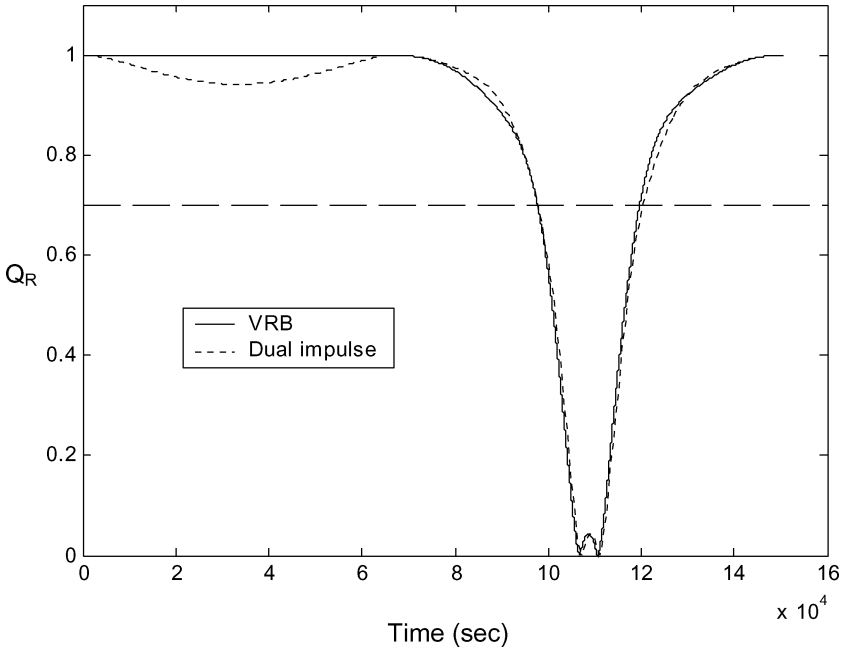

Fig. 12 Variation of Q_R throughout an entire orbit with the dual-impulse design.

Figure 12 shows the result of optimization over $(\lambda, \omega, V_x, V_y, V_z)$ for this dual-impulse solution, using the same cost-function weights $[w_1 = 0,\ w_3 = 1$ from Eq. (23)] as the VRB optimization. The last Table 4 column provides a comparison of the new dual-impulse and previous VRB solutions. The dual-impulse solution compares favorably, requiring roughly half the fuel of the VRB for its two impulses per spacecraft and enjoying the same total observation time per orbit given that $Q_{R,\min} = 0.7$. Although incapable of maintaining perfect geometry long-term, this result suggests that a dual- or multi-impulse solution is a promising compromise between VRB and natural-orbit designs that warrants further consideration for MMS and other proposed formation missions.

Conclusions

A hierarchical optimization method was applied to design a four-satellite tetrahedral formation in an elliptical geocentric orbit. To minimize search-space size in the natural-orbit case, geometric properties were exploited to derive a reduced set of design variables that describe the orientation ρ of each satellite's orbital plane. Natural orbits maintain near-regular geometries longest when individual spacecraft ρ match or are very similar. This is intuitive because satellite velocities are approximately in the same direction so long as separation distance is substantially smaller than the reference orbit semimajor axis.

A comparison between natural-orbit, VRB, and dual-impulse tetrahedral formation solutions shows that active satellite control substantially improves average quality factor and observation time per orbit at reasonable propellant cost. Natural-orbit formations have the indisputable advantage of requiring no active thrust for formation maintenance, but the formation geometry inevitably degrades as the satellites drift in their respective orbits. The result is that near-regular tetrahedra are maintained for only about 34% of the total orbit time, whereas the VRB and dual-impulse solutions provide high-quality data for over 85% of the orbit. Although the VRB is the only design capable of maintaining precise geometry long-term, the dual-impulse solution mitigates potential interference from thrusters and requires less fuel, suggesting a multi-impulse strategy as a promising avenue for further research.

For final mission design, however, the Keplerian motion assumption must be relaxed to include J_2 and other gravitational effects, the formation assembly problem (e.g., from launch to tetrahedron) must be addressed, and reconfiguration (e.g., new size) must be analyzed. The MMS formation must also be designed so that the assembled region precesses to follow the magnetosphere as the Earth orbits the Sun. Our tetrahedron results were primarily for satellite separations of 10 km. Although similar natural orbit results are found when satellite separations increase to 100 km and even 1000 km, VRB fuel expenditure increases substantially. As separation distance becomes a significant fraction of semimajor axis, both VRB and natural-orbit solutions vary in a manner not fully addressed by this work.

Acknowledgments

This work was partially supported under NASA Goddard Space Flight Center (GSFC) Grant NNG04GA64A. The authors thank Aaron Hoskins for his work on the dual-impulse solution, Rob Sanner and Yannick Pennecot of the University of Maryland for their collaborative efforts to develop the virtual rigid body concept, and Steve Hughes and others in the GSFC Flight Dynamics group for their invaluable feedback.

References

[1]Conkey, D., Dell, G., Good, S., and Bristow, J., "EO-1 Formation Flying Using Autocon^{TM}," *Proceedings of the IEEE Aerospace Conference*, Vol. 7, Inst. of Electrical and Electronics Engineers, Piscataway, NJ, 2000, pp. 55–61.

[2]Dow, J., Matussi, S., Dow, R. M., Schmidt, M., and Warhaut, M., "The Implementation of the Cluster II Constellation," *Acta Astronautica*, Vol. 54, No. 9, 2004, 0094-5765.

[3]Curtis, S., "The Magnetospheric Multiscale Mission Resolving Fundamental Processes in Space Plasmas," NASA TM2000-209883, NASA Goddard Space Flight Center, Dec. 2000.

[4]Curtis, S., Petruzzo, C., Clark, P., and Peterson., A., "The Magnetospheric Multi-Scale Mission: An Electronically Tethered Constellation of Four Spacecraft," Third International Workshop on Satellite Constellations and Formation Flying, Feb. 2003.

[5]Hughes, S. P., "Formation Tetrahedron Design for Phase I of the Magnetospheric Multiscale Mission," *Proceedings of the Flight Mechanics Symposium*, NASA Goddard Space Flight Center, Oct. 2003.

[6]Hughes, S. P., "Orbit Design for Phase I and II of the Magnetospheric Multiscale Mission," *Proceedings of the AAS 27th Rocky Mountain Guidance and Control Conference*, American Astronautical Society, San Diego, CA, 2004.

[7]Chichka, D. F., "Satellite Clusters with Constant Apparent Distribution," *Journal of Guidance, Control, and Dynamics*, Vol. 24, No. 1, 2001, pp. 117–122.

[8]DeCou, A. B., "Orbital Station-Keeping for Multiple Spacecraft Interferometry," *Journal of the Astronautical Sciences*, Vol. 39, No. 3, 1991, pp. 283–297.

[9]Hadaegh, F. Y., Lu, W.-M., and Wang, P. K. C., "Adaptive Control of Formation Flying Spacecraft for Interferometry," International Federation of Automatic Control Conf., July 1997.

[10]Siegel, A., and Blandino, J., "Propulsion Requirements and Options for Astronomical Imaging Formations in Earth Orbit," AIAA Paper 2003-4577, July 2003.

[11]Vassar, R. H., and Sherwood, R. B., "Formation Keeping for a Pair of Satellites in a Circular Orbit," *Journal of Guidance, Control, and Dynamics,* Vol. 8, No. 2, 1985, pp. 235–242.

[12]Surka, D., Brito, M., and Harvey, C., "Development of the Real-Time Object–Agent Flight Software Architecture for Distributed Satellite Systems," *Proceedings of the IEEE Aerospace Conference*, Inst. of Electrical and Electronics Engineers, Piscataway, NJ, 2001.

[13]Breger, L., Ferguson, P., How, J., Thomas, S., McLoughlin, T., and Campbell, M., "Distributed Control of Formation Flying Spacecraft Built on OA," AIAA Paper 2003-5366, Aug. 2003.

[14]Campbell, M., and Schetter, T., "Comparison of Multiple Agent-Based Organizations for Satellite Constellations," *Journal of Spacecraft and Rockets*, Vol. 39, No. 2, 2002, pp. 274–282.

[15]Ferguson, P., Yang, T.,Tillerson, M., and How, J., "New Formation Flying Testbed for Analyzing Distributed Estimation and Control Architectures," AIAA Paper 2002-4961, Aug. 2002.

[16]Sabol, C., Burns, R., and McLaughlin, C. A., "Satellite Formation Flying Design and Evolution," *Journal of Spacecraft and Rockets*, Vol. 38, No. 2, 2001, pp. 270–278.

[17]Koon, W., Marsden, J., and Murray, R., "J2 Dynamics and Formation Flight," AIAA Paper 2001-4090, Aug. 2001.

[18]Schweighart, S., and Sedwick, R., "A High Fidelity Linearized J2 Model for Satellite Formation Flight," *Journal of Guidance, Control, and Dynamics*, Vol. 25, No. 6, 2002, pp. 1073–1080.

[19]Schaub, H., and Alfriend, K. T., "J2 Invariant Relative Orbits for Spacecraft Formations," *Celestial Mechanics and Dynamical Astronomy*, Vol. 79, No. 2, 2001, pp. 77–95.

[20]Gim, D., and Alfriend, K., "State Transition Matrix of Relative Motion for the Perturbed Noncircular Reference Orbit," *Journal of Guidance, Control, and Dynamics*, Vol. 26, No. 6, 2003, pp. 956–971.

[21]Seereeram, S., Li, E., Ravichandran, B., Mehra, R., Smith, R., and Beard, R., "Multi-Spacecraft Formation Initialization using Genetic Algorithm Techniques," American Astronautical Society, AAS Paper 00-033, Feb. 2000.

[22]Richards, A., Schouwenaars, T., How, J., and Feron, E., "Spacecraft Trajectory Planning with Avoidance Constraints Using Mixed-Integer Linear Programming," *Journal of Guidance, Control, and Dynamics*, Vol. 25, No. 4, 2002, pp. 755–764.

[23]Campbell, M. E., "Planning Algorithm for Large Satellite Clusters," AIAA Paper 2002-4959, Aug. 2002.

[24]Jilla, C., and Miller, D., "Multi-Objective, Multidisciplinary Design Optimization Methodology for Distributed Satellite Systems," *Journal of Spacecraft and Rockets*, Vol. 41, No. 1, 2004, pp. 39–50.

[25]Ross, I. M., King, J. T., and Fahroo, F., "Designing Optimal Spacecraft Formations," AIAA Paper 2002-4635, Aug. 2002.

[26]Benjamin, J., and Pate-Cornell, M., "Risk Chair for Concurrent Design Engineering: Satellite Swarm Illustration," *Journal of Spacecraft and Rockets*, Vol. 41, No. 1, 2004, pp. 51–59.

[27]Engels, R., and Junkins, J., "The Gravity-Perturbed Lambert Problem: A KS Variation of Parameters Approach," *Celestial Mechanics*, Vol. 24, May 1981, pp. 3–21.

[28]Shen, H., and Tsiotras, P., "Optimal Two-Impulse Rendezvous Using Multiple-Revolution Lambert Solutions," *Journal of Guidance, Control, and Dynamics*, Vol. 26, No. 1, 2003, pp. 50–61.

[29]Alfriend, K. T., Schaub, H., and Gim, D. W., "Gravitational Perturbations, Nonlinearity and Circular Orbit Assumption Effects on Formation Flying Control Strategies," American Astronautical Society, AAS Paper 00-012, Feb. 2000.

[30]Wang, P. K. C., and Hadaegh, F. Y., "Coordination and Control of Multiple Microspacecraft Moving in Formation," *Journal of the Astronautical Sciences*, Vol. 44, No. 3, 1996, pp. 315–355.

[31]Guinn, J. P., "Precise Relative Motions of Formation Flying Space Vehicles," AIAA Paper 98-4187, Aug. 1998.

[32]Ren, W., and Beard, R., "Virtual Structure Based Spacecraft Formation Control with Formation Feedback," AIAA Paper 2002-4963, Aug. 2002.

[33]Penneçot, Y., Atkins, E., and Sanner, R., "Intelligent Spacecraft Formation Management and Path Planning," AIAA Paper 2002-1072, Jan. 2002.

[34]Atkins, E., and Penneçot, Y., "Autonomous Satellite Formation Assembly and Reconfiguration with Gravity Fields," *Proceedings of the IEEE Aerospace Conference* [CD-ROM], Inst. of Electrical and Electronics Engineers, Piscataway, NJ, 2002.

[35]Bate, R., Mueller, D., and White, J., *Fundamentals of Astrodynamics*, Dover, New York, 1971.

[36]Tsyganenko, N. A., "Modeling the Earth's Magnetospheric Magnetic Field Confined Within a Realistic Magnetopause," *Journal of Geophysical Research*, Vol. 100, No. A4, 1995, pp. 5599–5612.

[37]Chavez Clemente, D., *Hierarchical Optimization of Virtual Rigid Body Spacecraft Formations*, M.S. Thesis, Aerospace Engineering Dept., Univ. of Maryland, College Park, MD, Sept. 2003.

[38]Robert, P., Roux, A., Harvey, C., Dunlop, M., Daly, P., and Glassmeier, K.-H., "Tetrahedron Geometric Factors," *Analysis Methods for Multispacecraft Data*, edited by G. Paschmann and P. W. Daly, Chap. 13, ISSI Scientific Repts., No. SR-001, ESA Publ. Div., Noordwijk, The Netherlands, 1998, pp. 323–348.

[39]Daly, P., *The Tetrahedron Quality Factors of CSDS*, Max-Planck-Institut für Aeronomie, Heidelberg, Germany, 1994.

[40]Vallado, D. A., *Fundamentals of Astrodynamics and Applications*, Space Technology Library, 2nd ed., Kluwer Academic, Boston, 2001.

C. McLaughlin
Associate Editor